Int. J. Solids Structures, 1977, Vol. 13, pp. 675–681. Pergamon Press. Printed in Great Britain

DYNAMIC STRESS CONCENTRATION IN AN ELASTIC HALF SPACE WITH A SEMI-CIRCULAR CAVITY EXCITED BY SH WAVES

U. GAMER

I. Institut für Mechanik, Technische Universität Wien, 1040 Wien 4, Karlsplatz 13, Austria

(*Received* 4 *November* 1976)

Abstract—Subject of the investigation is the stress distribution and the dynamic stress concentration factor at the surface of a semi-circular cavity in a half space excited by plane harmonic SH waves. Using wave function expansion for the incident wave and the reflected waves, a closed form solution is obtained. Numerical results are represented graphically.

INTRODUCTION

As reviewed in a recent monograph[1], the determination of dynamic stress concentrations in solids is of primary importance in the study of dynamic strength of materials with inhomogeneity, and in the design of underground structures subject to ground blasting waves. Because of the difficulty in analysis, most known results are confined to inhomogeneities, like a cavity or a rigid insert, in an infinite space. Physically, this means that if, besides the inhomogeneity, there exists a bounding surface, the effect of the waves reflected from the bounding surface is neglected. This omittance is justifiable when the bounding surface is at a large distance from the inhomogeneity. For the case of a half space with a cavity on the surface as considered in this paper, the effect of scattering of waves by the cavity surface, and the effect of reflection from the plane boundary may be of equal importance, and they must be considered simultaneously.

Exact solutions for the scattering of elastic waves by a surface cavity of any shape on a semi-infinite solid are difficult to find. The only known results are the scattering of SH waves by a semi-circular elastic cylinder[2, 3], or a half elliptical rigid cylinder[4]. The former includes the case of a rigid circular cylinder as first obtained by Luco[5]. In this paper, we investigate the case of a semi-circular cylindrical cavity in detail.

The solution is derived by the method of series expansion in terms of wave functions in polar coordinates (see [1], Chaps. 2 and 3). The exact series solution can be evaluated numerically with great accuracy for the case of an incident wave with wave length not too small.

For the purpose of understanding the effect of the plane boundary on the stress concentrations, we calculated the dynamic stresses at the surface of the cavity due to an incident plane harmonic SH wave. As expected, a change of the angle of emergence, γ, which ranges from 0 to $\pi/2$ alters significantly the dynamic stress concentrations. The case of grazing incidence ($\gamma = 0$) where the direction of the wave normal is parallel to the plane boundary is the same as the case of a circular cylindrical cavity in an infinite space with the same incident wave. The case of normal incidence ($\gamma = \pi/2$) where the propagation vector is perpendicular to the plane differs significantly from the case of grazing incidence. For oblique incidence, the dynamic stress concentration at high frequencies may be higher than that at low frequencies. This result is unexpected and merits further consideration in the study of transient waves.

SERIES SOLUTION IN WAVE FUNCTIONS

Consider the propagation of a horizontally polarized shear wave (SH wave) in a half space the plane boundary of which is the $z-x$ coordinate plane (Fig. 1). The displacement w of simple harmonic waves with a time factor $\exp(-i\omega t)$ satisfies the two dimensional scalar wave equation

$$(\nabla^2 + k^2)w(x, y) = 0 \tag{1}$$

where the wave number $k = \omega/c$, and ω is the circular frequency, and c the shear wave speed. The non vanishing stress components are

$$\sigma_{xz} = \mu \frac{\partial w}{\partial x}, \qquad \sigma_{yz} = \mu \frac{\partial w}{\partial y} \tag{2}$$

where μ is the shear modulus of the material. In polar coordinates (r, θ),

$$\sigma_{rz} = \mu \frac{\partial w}{\partial r}, \qquad \sigma_{\theta z} = \mu \frac{1}{r} \frac{\partial w}{\partial \theta}. \tag{3}$$

For a traction free boundary ($y = 0$), the incident wave, $w^{(i)}$, and the reflected wave, $w^{(r)}$, may be represented by

$$w^{(i),(r)} = w_0 \exp [ik(x \cos \gamma \pm y \sin \gamma)] \tag{4}$$

where w_0 indicates the displacement amplitude, and γ is the angle of emergence (Fig. 1). The resultant wave in the half space is

$$w^{(i)} + w^{(r)} = 2w_0 \cos (ky \sin \gamma) \, e^{ikx \cos \gamma} \tag{5}$$

or in polar coordinates,

$$w^{(i)} + w^{(r)} = 2w_0 \sum_{n=0}^{\infty} \epsilon_n i^n J_n(kr) \cos n\gamma \cos n\theta. \tag{6}$$

The above result can easily be derived by first noting that $x \cos \gamma \pm y \sin \gamma = r \cos (\theta \pm \gamma)$, and then applying the expansion formula for each of the plane waves in (4) into a series of wave functions (1). The ϵ_n in (6) equals 1 when $n = 0$, and equals 2 when $n = 1, 2, 3 \ldots J_n(kr)$ is the Bessel function of the first kind.

With a semi-circular cavity of radius a in the half space, the incident wave is further scattered by the cavity. We represent the scattered waves by

$$w^{(s)} = 2w_0 \sum_{n=0}^{\infty} A_n H_n(kr) \cos n\theta \tag{7}$$

where $H_n(kr) = J_n(kr) + iY_n(kr)$ is the Hankel function of the first kind. The unknown coefficients A_n are determined from the boundary condition

$$\sigma_{rz} = 0 \quad \text{at} \quad r = a. \tag{8}$$

The total wave in the half space with a cavity is

$$w = w^{(i)} + w^{(r)} + w^{(s)}, \tag{9}$$

and the boundary condition (8) is satisfied if

$$A_n = -\epsilon_n i^n [J_n'(ka)/H_n'(ka)] \cos n\gamma \tag{10}$$

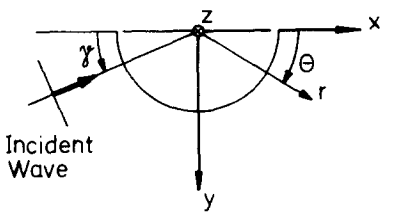

Fig. 1. Half space with semi-circular cavity.

where a prime denotes differentiation with respect to the argument. The complete solution is given by the sum of (5) and (7) while A_n is given by (10).

DYNAMIC STRESS CONCENTRATIONS

For the investigation of stress concentration, we evaluate the shear stress $\sigma_{\theta z}$ at the boundary $r = a$ according to

$$\frac{\sigma_{\theta z}}{2\sigma_0} = -\frac{2}{kr}\sum_{n=1}^{\infty} ni^n\left[J_n(kr) - \frac{J_n'(ka)}{H_n'(ka)}H_n(kr)\right]\cos n\gamma \sin n\theta \tag{11}$$

with $\sigma_0 = \mu k w_0$. Since $\sigma_{rz} = 0$ at $r = a$, the absolute value $|\sigma_{\theta z}(a, \theta)|$ is the largest principal stress at the cavity surface in one complete cycle of the incident wave.

Substituting the Bessel functions by their asymptotic formulae for small argument ka (see, e.g. [5]), one obtains

$$\frac{|\sigma_{\theta z}|}{2\sigma_0} = 2\cos\gamma \sin\theta. \tag{12}$$

In a polar coordinate system $(|\sigma_{\theta z}|/2\sigma_0, \theta)$, this function is a circle of diameter $2\cos\gamma$. $ka \to 0$ means either static limit, i.e. infinite wave length, or an infinitesimal notch. (In Figs. 2 and 3, these circles have been omitted for the sake of clarity.)

To compare $\sigma_{\theta z}(a, \theta)$ with the principal stresses at the corresponding points (a, θ) in the absence of a cavity we must restore the time factor $\exp(-i\omega t)$ in (5). According to (2), the stresses at every point (x, y) due to the combined incident and reflected waves are

$$\begin{aligned}\sigma_{xz}^{(i+r)} &= -2\sigma_0 \cos\gamma \cos(ky \sin\gamma)\sin(kx\cos\gamma - \omega t),\\ \sigma_{yz}^{(i+r)} &= -2\sigma_0 \sin\gamma \sin(ky\sin\gamma)\cos(kx\cos\gamma - \omega t).\end{aligned} \tag{13}$$

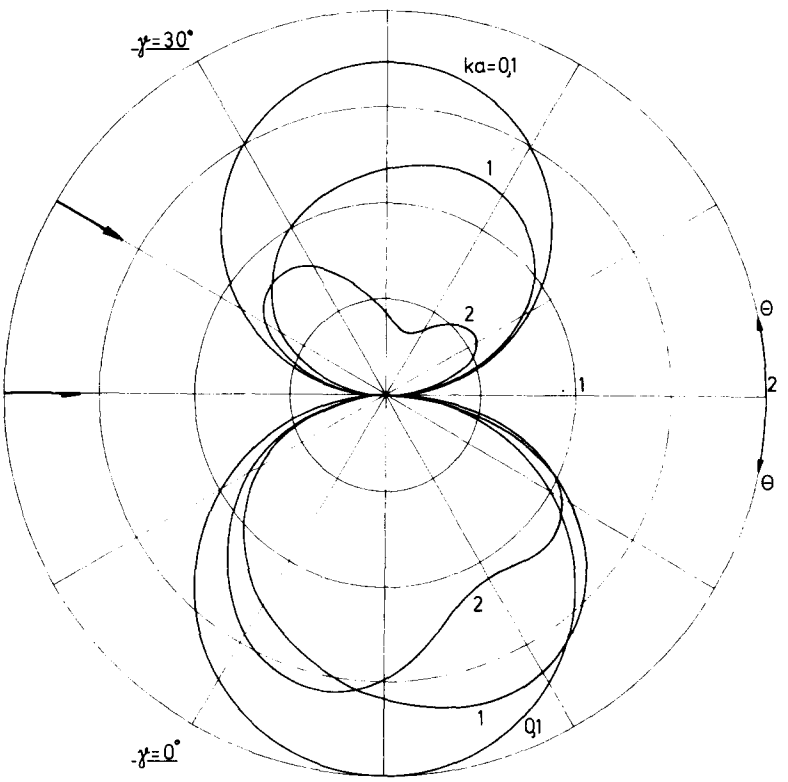

Fig. 2. Nondimensional stress amplitude as a function of the angle of observation.

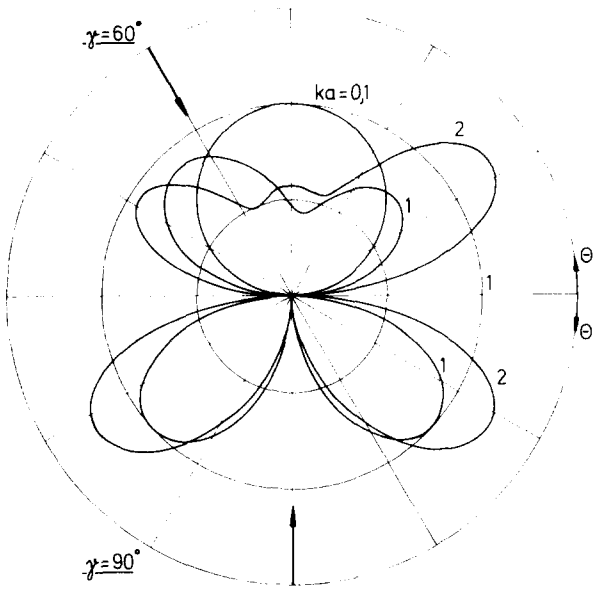

Fig. 3. Nondimensional stress amplitude as a function of the angle of observation.

During one complete cycle $2\pi/\omega$ of wave motion, the peak values of these two stresses do not occur at the same instant. Note that when all the stress components but σ_{xz} and σ_{yz} vanish, two of the principal stresses are $\pm\sigma$, and the third equals zero, where

$$\sigma = (\sigma_{xz}^2 + \sigma_{yz}^2)^{1/2}. \tag{14}$$

Thus, in one complete cycle, the σ_{max} in the undisturbed medium (half space without cavity) may be either σ_1 or σ_2 where

$$\begin{aligned} \sigma_1 &= 2\sigma_0 \cos\gamma \cos(ky \sin\gamma), \\ \sigma_2 &= 2\sigma_0 \sin\gamma \sin(ky \sin\gamma). \end{aligned} \tag{15}$$

Their magnitudes depend on the location y, wave length $2\pi/k$, and the angle of emergence γ.

We now define the dynamic stress concentration factor (*DSCF*) as

$$DSCF = \frac{|\sigma_{\theta z}(a, \theta)|}{\sigma_{1,2}(a, \theta)} \tag{16}$$

where $\sigma_{1,2}$ is given by (15) with $y = a \sin\theta$. The larger of the two stresses, σ_1 and σ_2, should be used to calculate the *DSCF*. When $\gamma = 0$, the *DSCF* for the half space with a semi-circular cylinder is the same as that for an infinite space with a complete cylindrical hole under the influence of a plane *SH* wave. The case of $\gamma = \pi/2$ gives rise to a maximum stress $\sigma_2 = 2\sigma_0 \sin ky$ in the undisturbed half space. At the nodal lines $y = n\pi/k$ ($n = 0, 1, 2 \ldots$) resulting from the interference of the incident and reflected waves, $\sigma_2 = 0$. However, $|\sigma_{\theta z}|$ at the same location of the half space with a cavity does not always vanish on account of the additional interference with the scattered waves, and the ratio $|\sigma_{\theta z}|/\sigma_2 \to \infty$. Since this result is misleading we shall not define the *DSCF* for the case of $\gamma = \pi/2$ (normal incidence).

RESULTS

The distributions of $|\sigma_{\theta z}|/2\sigma_0$ as functions of θ are shown for $ka = 0.1, 1, 2$ for $\gamma = 0$ and 30° in Fig. 2, and for $\gamma = 60$ and 90° in Fig. 3. The curve for $ka = 0.1$ has been omitted in the lower half of Fig. 3 ($\gamma = 90°$). Also as functions of θ, Figs. 4 and 5 exhibit $|\sigma_{\theta z}|/2\sigma_0$ for $ka = 10$ with parameters $\gamma = 0$ and 30°, or $\gamma = 60$ and 90°, respectively. Variations of $|\sigma_{\theta z}|/2\sigma_0$ as continuous

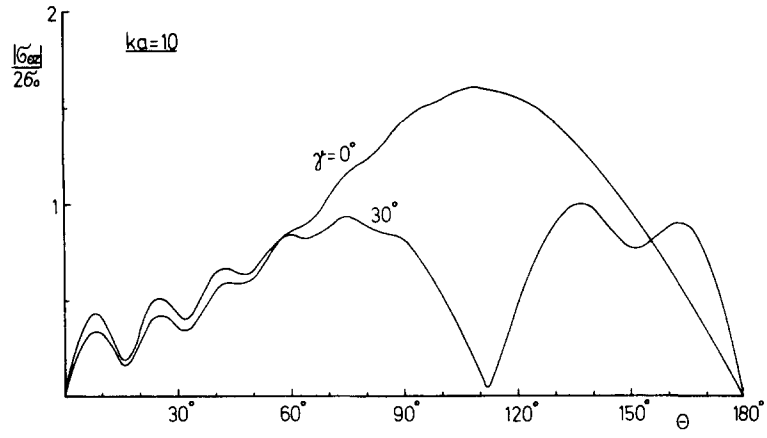

Fig. 4. Nondimensional stress amplitude plotted vs the angle of observation.

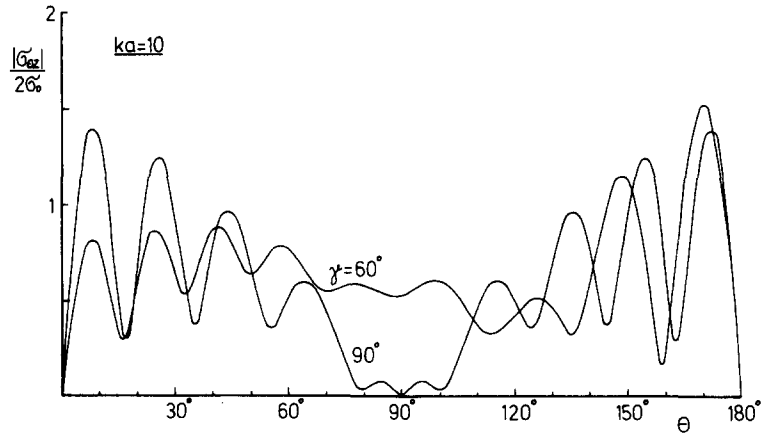

Fig. 5. Nondimensional stress amplitude plotted vs the angle of observation.

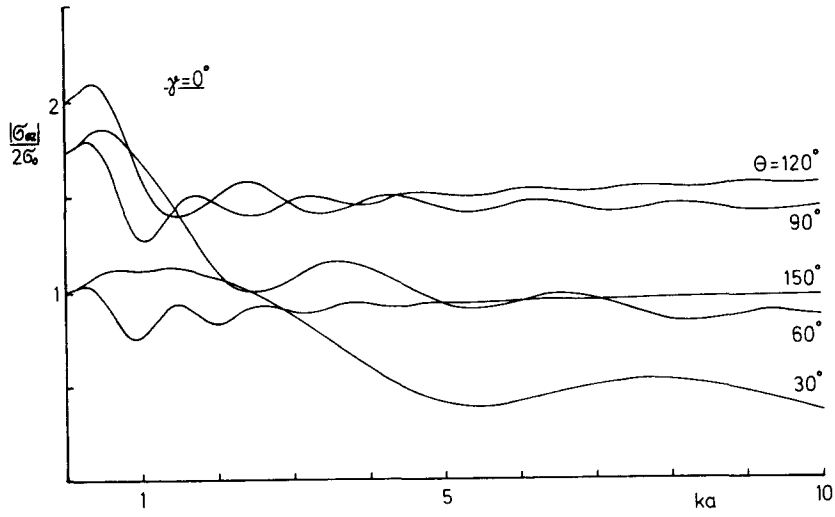

Fig. 6. Nondimensional stress amplitude plotted vs the nondimensional wave number.

functions of ka are shown in Figs. 6–8 for the angles of emergence $\gamma = 0, 30, 60°$, respectively, and the angles of observation $\theta = 30, 60, 90, 120, 150°$ as parameters. In Fig. 7 ($\gamma = 30°$), the angle of observation $\theta = 175°$ has been added. In Fig. 9, stress is represented for $\gamma = 90°$ and $\theta = 30$ and 60°.

The curves for $\gamma = 0°$ in Fig. 2 are known from the case of infinite space with circular cylinder[1]. Very similar to them are the curves for $\gamma = 30°$ presented in the upper half of Fig. 2. Figure 3 exhibits the interesting fact that dynamic stress ($ka = 2$) is essentially larger than static stress in the shadow zone as well as in the illuminated region. In the $\gamma = 90°$ case, there does not exist a limit $ka \to 0$. Figure 5 shows very high dynamic stresses ($ka = 10$) for $\gamma = 60°$ at the angle $\theta \approx 170°$, and for $\gamma = 90°$ at the angles $\theta \approx 10°$ and $\theta \approx 170°$.

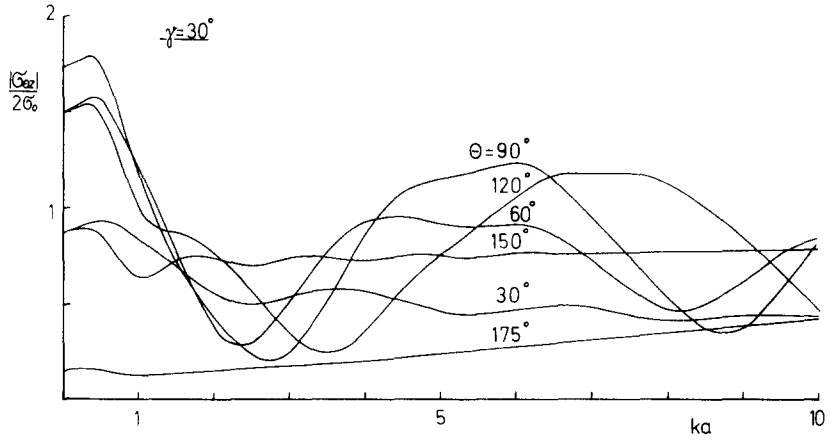

Fig. 7. Nondimensional stress amplitude plotted vs the nondimensional wave number.

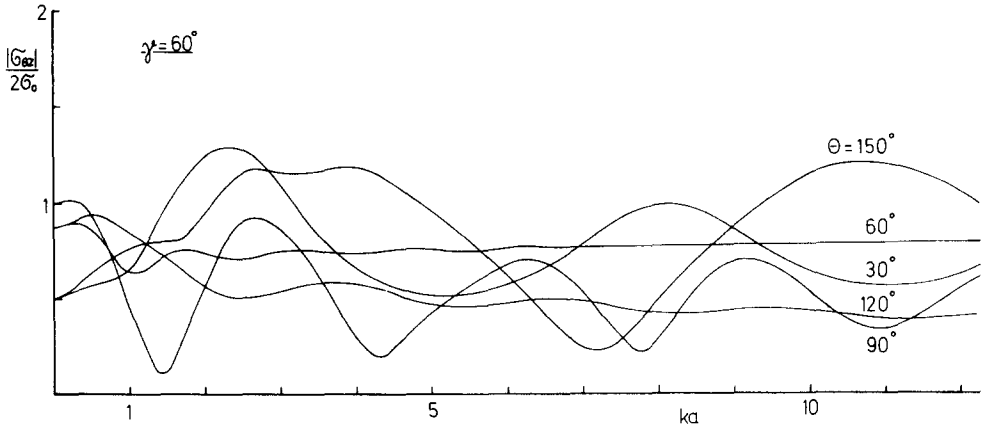

Fig. 8. Nondimensional stress amplitude plotted vs the nondimensional wave number.

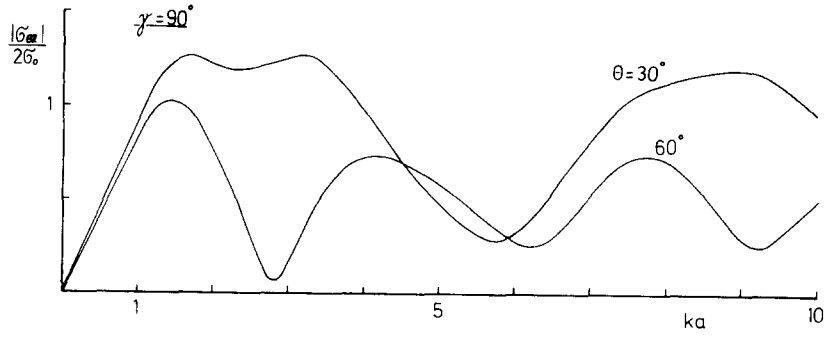

Fig. 9. Nondimensional stress amplitude plotted vs the nondimensional wave number.

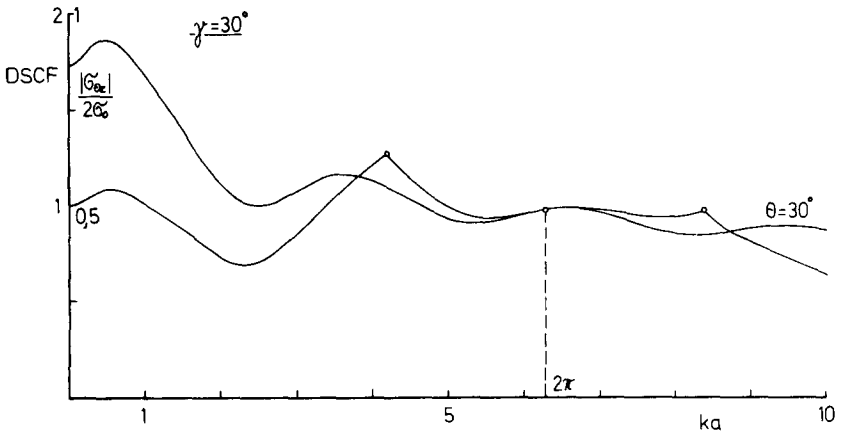

Fig. 10. Nondimensional stress amplitude and dynamic stress concentration factor plotted vs the nondimensional wave number.

Figure 6 shows the well known fact of stress becoming smaller with increasing frequency in the shadow zone; there is no influence of the free surface of the half space. Figure 7 shows considerable re-increases after previous decreases. For $\theta = 175°$, in the range under consideration, after a small decrease, the stress increases monotonously with ka. The most striking feature in Fig. 8 is the observation that, for $\theta = 150°$, the second peak exceeds the first one.

As an example for the *DSCF*, Fig. 10 shows this quantity, and in a twice as large scale, the non dimensional stress as a function of ka for $\gamma = 30°$ and $\theta = 30°$. The corners in the *DSCF* stem from the fact that, as mentioned, in calculating the *DSCF* according to the definition (16), the larger of the two stresses (15) has to be inserted. At the angle of observation $\theta = 30°$, for $ka = 4.2$, the principal stress in the half space with cavity is 26% larger than the corresponding stress in the undisturbed half space.

Acknowledgement—The author is very much indebted to Professor Y.-H. Pao of Cornell University, Ithaca, N.Y., for fruitful discussions.

REFERENCES

1. Y.-H. Pao and C.-C. Mow, *Diffraction of Elastic Waves and Dynamic Stress Concentration*. Crane Russak, New York (1973).
2. M. D. Trifunac, Surface motion of a semi-cylindrical Alluvial valley for incident plane *SH* waves. *Bull. Seismological Soc. Am.* **61**, 1755–1770 (1971).
3. U. Gamer and Y.-H. Pao, Wechselwirkung zwischen Halbraum und Halbzylinder bei Erregung durch eine ebene harmonische SH-Welle. *ZAMM* **55**, T81–T84 (1975).
4. H. L. Wong and M. D. Trifunac, Interaction of a shear wall with the soil for incident plane *SH* waves: elliptical rigid foundation. *Bull. Seismological Soc. Am.* **64**, 1825–1842 (1974).
5. J. E. Luco, Dynamic Interaction of a Shear Wall with the Soil, *J. Engng Mech. Div. ASCE*, **95**(EM2), Proc. Paper 6497, 333–346 (1969).
6. M. Abramowitz and I. A. Stegun, *Handbook of Mathematical Functions*. Dover, New York (1965).